Self-Assembly and Phase Behavior of Germanium Oxide Nanoparticles in Basic Aqueous Solutions

Jeffrey D. Rimer, Daniel D. Roth, Dionisios G. Vlachos,* and Raul F. Lobo*

Center for Catalytic Science and Technology, Department of Chemical Engineering, University of Delaware, Newark, Delaware 19716

Received September 26, 2006. In Final Form: November 20, 2006

We show that germania nanoparticle self-assembly in basic aqueous solutions occurs at a critical aggregation concentration (CAC) corresponding to a 1:1 GeO_2/OH^- molar ratio. A combination of pH, conductivity, and small-angle X-ray scattering (SAXS) measurements was used to monitor the effect of incremental additions of germanium (IV) ethoxide to basic solutions of sodium hydroxide or tetraalkylammonium cations. Plots of pH versus total germania concentration at varying alkalinities generated a phase diagram with three distinct regions. The diagram was analyzed with a thermodynamic model based on the chemical equilibria of germania speciation and dissociation. The model, which uses the GeO−H dissociation constant ($pK = 7.1$) as the single fitting parameter, quantitatively captures trends in the CAC and pH. SAXS patterns reveal that the germania nanoparticles have either a cubic or a spherical geometry of dimension ∼1 nm that is independent of solution pH and cation. On the basis of these and other literature findings, we propose that the germania nanoparticle structure is that of the cubic octamer (double four-membered ring, $Ge_8O_{12}(OH)_8$), which is common among condensed GeO_2 materials and building units in [Ge,Si]-zeolites. Comparisons between germania and silica solutions show distinct differences in their phase behavior and nanoparticle structure. The results presented here, in combination with previous studies of siliceous solutions, provide a framework for ongoing studies of combined germania-silica phase behavior, which is part of an overarching effort to understand the influence of heteroatoms in the growth and structure direction of zeolites.

1. Introduction

The unique properties of germanium have led to the development of Ge-containing zeolites, with over 20 framework types reported in the literature. The incorporation of Ge in the zeolite framework drives the formation of large (12-membered rings, MR) and extra-large (> 12-MR) pores or channels. Subsequently, these materials could find extensive use in petroleum refining, ion exchange, and separations, due to the increased accessibility by larger molecules. In particular, microporous materials with open framework structures have received much attention for their widespread potential in separations of large molecules, such as heavy oils and pharmaceuticals.[1] Corma and co-workers synthesized a series of [Si,Ge]-zeolites with an ISV framework type consisting of large channels, with unique properties for applications in oil refinery and petrochemical processes.[2] In addition, Ge-zeolites have shown potential for enhancing catalytic activity, particularly in ZSM-5 catalysts where Ge incorporation reduces deactivation by introducing a higher mesoporosity and leads to a greater number of defects (i.e., hydroxyl groups) without altering the overall topology.[3]

Germanium has been incorporated into both mesoporous materials[4,5] as well as numerous zeolitic frameworks: MFI;[3,6−10] AST;[11] BEC and LTA;[12] UOZ;[13] EUO;[14] RHO, NAT, GIS, and FAU;[15] BEA;[16,17] and the UCSB series.[18−20] A significant amount of effort has been focused on incorporating Ge into the ITQ series.[2,14,21−28] The presence of Ge causes an expansion of the unit cell, without significantly affecting the zeolite acidity.[6] Many studies have focused on the Ge/Si ratio, where it is found that in some zeolites (e.g., MFI framework), isomorphic substitution

* Corresponding authors. (R.F.L.) Tel.: (302) 831-1261; e-mail: lobo@che.udel.edu. (D.G.V.) Tel.: (302) 831-2830; e-mail: vlachos@che.udel.edu.

(1) Zhou, Y. M.; Zhu, H. G.; Chen, Z. X.; Chen, M. Q.; Xu, Y.; Zhang, H. Y.; Zhao, D. Y. *Angew. Chem., Intl. Ed.* **2001**, *40*, 2166.
(2) Corma, A.; Diaz-Cabanas, M. J.; Fornes, V. *Angew. Chem., Intl. Ed.* **2000**, *39*, 2346.
(3) van de Water, L. G. A.; van der Waal, J. C.; Jansen, J. C.; Maschmeyer, T. *J. Catal.* **2004**, *223*, 170.
(4) Lu, Q. Y.; Gao, F.; Li, Y. Q.; Zhou, Y. M.; Zhao, D. Y. *Micropor. Mesopor. Mater.* **2002**, *56*, 219.
(5) Zou, X. D.; Conradsson, T.; Klingstedt, M.; Dadachov, M. S.; O'Keeffe, M. *Nature* **2005**, *437*, 716.
(6) van de Water, L. G. A.; van der Waal, J. C.; Jansen, J. C.; Cadoni, M.; Marchese, L.; Maschmeyer, T. *J. Phys. Chem. B* **2003**, *107*, 10423.
(7) van de Water, L. G. A.; Zwijnenburg, M. A.; Sloof, W. G.; van der Waal, J. C.; Jansen, J. C.; Maschmeyer, T. *Chem. Phys. Chem.* **2004**, *5*, 1328.
(8) Kosslick, H.; Tuan, V. A.; Fricke, R.; Peuker, C.; Pilz, W.; Storek, W. *J. Phys. Chem.* **1993**, *97*, 5678.
(9) Li, S.; Tuan, V. A.; Falconer, J. L.; Noble, R. D. *Micropor. Mesopor. Mater.* **2003**, *58*, 137.
(10) Tuan, V. A.; Falconer, J. L.; Noble, R. D. *Micropor. Mesopor. Mater.* **2000**, *41*, 269.
(11) O'Keeffe, M.; Yaghi, O. M. *Chem.−Eur. J.* **1999**, *5*, 2796.
(12) Sastre, G.; Pulido, A.; Corma, A. *Micropor. Mesopor. Mater.* **2005**, *82*, 159.
(13) Mathieu, Y.; Paillaud, J. L.; Caullet, P.; Bats, N. *Micropor. Mesopor. Mater.* **2004**, *75*, 13.
(14) Sastre, G.; Pulido, A.; Castaneda, R.; Corma, A. *J. Phys. Chem. B* **2004**, *108*, 8830.
(15) Johnson, G. M.; Tripathi, A.; Parise, J. B. *Chem. Mater.* **1999**, *11*, 10.
(16) Corma, A.; Navarro, M. T.; Rey, F.; Rius, J.; Valencia, S. *Angew. Chem., Intl. Ed.* **2001**, *40*, 2277.
(17) Corma, A.; Navarro, M. T.; Rey, F.; Valencia, S. *Chem. Commun.* **2001**, 1486.
(18) Bu, X. H.; Feng, P. Y.; Stucky, G. D. *J. Am. Chem. Soc.* **1998**, *120*, 11204.
(19) Bu, X. H.; Feng, P. Y.; Stucky, G. D. *Chem. Mater.* **2000**, *12*, 1505.
(20) Gier, T. E.; Bu, X. H.; Feng, P. Y.; Stucky, G. D. *Nature* **1998**, *395*, 154.
(21) Corma, A.; Diaz-Cabanas, M. J.; Garcia, H.; Palomares, E. *Chem. Commun.* **2001**, 2148.
(22) Blasco, T.; Corma, A.; Diaz-Cabanas, M. J.; Rey, F.; Vidal-Moya, J. A.; Zicovich-Wilson, C. M. *J. Phys. Chem. B* **2002**, *106*, 2634.
(23) Corma, A.; Puche, M.; Rey, F.; Sankar, G.; Teat, S. J. *Angew. Chem., Intl. Ed.* **2003**, *42*, 1156.
(24) Corma, A.; Diaz-Cabanas, M. J.; Rey, F.; Nicolooulas, S.; Boulahya, K. *Chem. Commun.* **2004**, 1356.
(25) Alvaro, M.; Atienzar, P.; Corma, A.; Ferrer, B.; Garcia, H.; Navarro, M. T. *J. Phys. Chem. B* **2005**, *109*, 3696.
(26) Blasco, T.; Corma, A.; Diaz-Cabanas, M. J.; Rey, F.; Rius, J.; Sastre, G.; Vidal-Moya, J. A. *J. Am. Chem. Soc.* **2004**, *126*, 13414.
(27) Castaneda, R.; Corma, A.; Fornes, V.; Rey, F.; Rius, J. *J. Am. Chem. Soc.* **2003**, *125*, 7820.
(28) Corma, A.; Rey, F.; Rius, J.; Sabater, M. J.; Valencia, S. *Nature* **2004**, *431*, 287.

10.1021/la062828q CCC: $37.00
Published on Web 01/23/2007

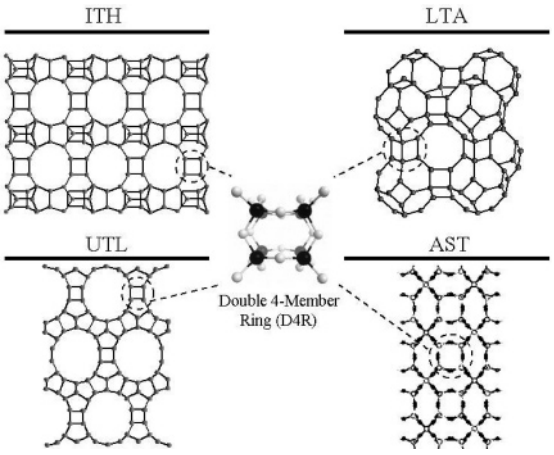

Figure 1. Zeolitic frameworks with double four-membered ring subunits for ITH,[23] UTL,[29] LTA,[30,31] and AST.[11]

of germanium can replace more than 30% of the silicon atoms, with an upper limit of 12.8 per unit cell.[8] In materials such as ITQ-7, it has been suggested by Blasco et al. that a maximum of two or three Ge atoms can occupy a double four-membered ring (D4R).[22]

The probability of forming frameworks with D4R subunits is greatly enhanced by the presence of Ge,[23,27,28,32−34] due to the increase in bond flexibility, since the optimum Ge−O−Ge bond angle of 130° is smaller than the 145° angle of the Si−O−Si bond,[11,25] as well as the longer Ge−O distance.[35] Figure 1 shows examples of various Ge-zeolite frameworks comprised of D4R subunits and represents only a fraction of those reported in the literature. Others include work by Corma et al., who showed that Ge stabilizes BEC (polymorph C of beta zeolite) by occupying positions in the D4R.[16] In the case of ITQ-7, Blasco et al. showed that Ge stabilizes the D4R but that crystallization is controlled by two opposing effects: cage stabilization from the presence of Ge atoms and the overall structural destabilization generated from geometric distortions.[22] In addition, it is generally found that an increasing concentration of germanium strongly influences zeolite growth by accelerating both nucleation and the rate of crystallization,[21−23,26,36] whereas incorporation of Ge in the framework causes an increase in zeolite metastability (i.e., an increase in the enthalpy of formation relative to the non-substituted zeolite).[35,37]

In addition to zeolitic D4R, pure germania solutions have been shown to form cubic eight-membered species. Cotton and Wilkinson report that the major ionic species in dilute aqueous solutions of GeO_2 appear to be $Ge(OH)_3O^-$, $Ge(OH)_2O_2^{2-}$, and $\{[Ge_8(OH)_4]_8(OH)_3\}^{3-}$.[38] However, the octameric cube is not limited to a Ge-containing species. The subunits for LTA (zeolite A) are D4R containing both aluminum and silicon atoms. The structure-directing agent for LTA synthesis is tetramethylammonium (TMA^+)—a molecule that has also been identified as being a unique component in the self-assembly of silica into cubic octamers.[39−42]

Much of the work done on Ge-zeolites has been focused on structural characterization, but the effects of germanium on the kinetics and mechanism of zeolite growth are not well-understood. There lacks a systematic study of the aqueous chemistry of germania and germania-silica solutions, which is needed to develop insight into the effects of Ge incorporation for the rational design of new materials. In this paper, we focus on all-germania aqueous solutions and present an analysis of the phase behavior through a combination of pH, conductivity, and small-angle X-ray scattering (SAXS) measurements. A chemical equilibrium model, based on germania dissociation and condensation, is used to predict both the phase diagram and the onset of nanoparticle self-assembly. The results of these analyses serve as a basis for studying mixed Ge/Si phase behavior, thereby providing a foundation for future mechanistic studies of [Ge,Si]-zeolite crystallization.

2. Experimental Procedures

Germania nanoparticles in basic solutions of monovalent cations were synthesized by first diluting concentrated tetramethylammonium hydroxide (TMAOH, 25% w/w, Alfa Aesar), tetrapropylammonium hydroxide (TPAOH, 40% w/w, Alfa Aesar), or sodium hydroxide in deionized water. Solutions of the latter were obtained by diluting a 5.0 M stock solution of sodium hydroxide (NaOH, Aldrich, pellets, 97+ %, ACS) to attain the desired alkalinity. After mixing for ~30 min, germanium (IV) ethoxide (99.95+%, Aldrich) was added to each solution, and the resulting mixture was vigorously stirred for at least 12 h prior to analysis. Molar compositions of *Y* GeO2/*X* M^+OH^-/9500 H_2O/4*Y* EtOH were prepared, with $Y = 0-75$, $X =$ 4, 9, 18, and 27, and $M^+ = Na^+$, TMA^+, and TPA^+. For each inorganic and organic cation, compositions above and below the 1:1 GeO_2/M^+OH^- molar ratio were chosen for analysis. Conductivity measurements were obtained with a VWR Model 2052 EC Meter, and the pH was measured using a Corning 355 pH/ion analyzer and a WTW SenTix 61 pH combination electrode. The pH meter was calibrated with standardized pH 7, 10, and 12 buffer solutions (Alfa Aesar).

SAXS experiments were conducted on a SAXSess (Anton-Paar) system. Samples were placed in a vacuum-tight 1 mm diameter quartz capillary holder and measured at 25 °C. A monochromatic, line-collimation source of Cu Kα radiation ($\lambda = 1.54$ Å) was used with a 265-mm sample-to-detector distance. The scattering patterns were collected over a 30 min period on a phosphor imaging plate within the *q*-range $0.1-8$ nm^{-1}. Patterns were normalized to the height of the primary beam signal using the SAXSquant software, and the signal from a normalized background solution (i.e., *X* M^+-OH^-/9500 H_2O) was subtracted from each nanoparticle sample. Analyses of patterns were performed according to procedures outlined in ref 43.

3. Chemical Equilibrium Model

Germanium (IV) ethoxide, $Ge(OC_2H_5)_4$, when added to water undergoes hydrolysis to form germanic acid, $Ge(OH)_4$

$$Ge(OC_2H_5)_4 + 4H_2O \leftrightarrow Ge(OH)_4 + 4C_2H_5OH \quad (1)$$

In basic solutions, germanic acid has been shown to exhibit two

(29) Paillaud, J. L.; Harbuzaru, B.; Patarin, J.; Bats, N. *Science* **2004**, *304*, 990.
(30) Sathupunya, M.; Gulari, E.; Wongkasemjit, S. *J. Eur. Ceram. Soc.* **2003**, *23*, 1293.
(31) Li, H. L.; Yaghi, O. M. *J. Am. Chem. Soc.* **1998**, *120*, 10569.
(32) Villaescusa, L. A.; Lightfoot, P.; Morris, R. E. *Chem. Commun.* **2002**, 2220.
(33) Zwijnenburg, M. A.; Bromley, S. T.; Jansen, J. C.; Maschmeyer, T. *Microporous Mesoporous Mater.* **2004**, *73*, 171.
(34) Wang, Y. X.; Song, J. Q.; Gies, H. *Solid State Sci.* **2003**, *5*, 1421.
(35) Li, Q. H.; Navrotsky, A.; Rey, F.; Corma, A. *Micropor. Mesopor. Mater.* **2003**, *64*, 127.
(36) Burton, A. W.; Zones, S. I.; Elomari, S. *Curr. Opin. Colloid Interface Sci.* **2005**, *10*, 211.
(37) Li, Q. H.; Navrotsky, A.; Rey, F.; Corma, A. *Micropor. Mesopor. Mater.* **2004**, *74*, 87.
(38) Cotton, F. A.; Wilkinson, G. *Advanced Inorganic Chemistry*, 5th ed.; Wiley: New York, 1988.
(39) Kinrade, S. D.; Swaddle, T. W. *Inorg. Chem.* **1988**, *27*, 4253. Kinrade, S. D.; Knight, C. T. G.; Pole, D. L.; Syvitski, R. T. *Inorg. Chem.* **1998**, *37*, 4272−4277. Kinrade, S. D.; Knight, C. T. G.; Pole, D. L.; Syvitski, R. T. *Inorg. Chem.* **1998**, *37*, 4278−4283.
(40) Burkett, S. L.; Davis, M. E. *Chem. Mater.* **1995**, *7*, 1453.
(41) Caratzoulas, S.; Vlachos, D. G.; Tsapatsis, M. *J. Phys. Chem. B* **2005**, *109*, 10429.
(42) Caratzoulas, S.; Vlachos, D. G.; Tsapatsis, M. *J. Am. Chem. Soc.* **2006**, *128*, 596.
(43) Rimer, J. D.; Vlachos, D. G.; Lobo, R. F. *J. Phys. Chem. B* **2005**, *109*, 12762.

dissociations

$$GeO_{(i-1)}(OH)_{(5-i)}^{(i-1)-} \overset{K_a^i}{\longleftrightarrow} GeO_i(OH)_{(4-i)}^{i-} + H^+,\ i = 1, 2 \quad (2)$$

where pK_a^1 and pK_a^2 at 25 °C are 9.3 and 12.4, respectively.[44] In addition, the dissociation of water must also be accounted for ($pK_w = 14$ at 25 °C)

$$H_2O \overset{K_w}{\longleftrightarrow} OH^- + H^+ \quad (3)$$

Germania condenses to form larger oligomeric species or nanoparticles. The overall reaction for the condensation to a bulk solid is ($\Delta G_c = -7.8$ kJ/mol)[44]

$$Ge(OH)_{4,(aq)} \overset{\Delta G_c}{\longleftrightarrow} GeO_{2,(s)} + 2H_2O \quad (4)$$

As will be discussed later in this paper, the most probable structure of the germania nanoparticle is that of a cubic octamer, $Ge_8O_{12}(OH)_8$, which contains eight Ge−OH bonds. Thus, eq 4 is rewritten as

$$Ge(OH)_4 \overset{K_{c,8}}{\longleftrightarrow} \frac{1}{8}Ge_8O_{12}(OH)_8 + \frac{3}{2}H_2O \quad (5)$$

The $GeO_{2,(s)}$ species in eq 4 is composed entirely of Ge−O−Ge bonds, while the germania octamer consists of 75% Ge−O−Ge bonds and 25% Ge−OH bonds. Therefore, the equilibrium constant, $K_{c,8}$, for the germania octamers is estimated from ΔG_c using the expression

$$K_{c,8} = \exp\left(\frac{-0.75\Delta G_c}{RT}\right) \quad (6)$$

where $pK_{c,8} = -1.02$ at 25 °C. In basic solutions, the Ge−octamer can also undergo a series of dissociation reactions

$$Ge_8O_{(11+i)}(OH)_{(9-i)}^{(i-1)-} \overset{K_{as}^i}{\longleftrightarrow} Ge_8O_{(12+i)}(OH)_{(8-i)}^{i-} + H^+,\ i = 1, 2,...,8 \quad (7)$$

In the absence of ^{73}Ge NMR data to identify species in solution, we assume that soluble germania is in the form of monomers that can only undergo a single dissociation. Thus, the total concentration of germanium, $[GeO_2]$, is present as monomeric species, $[GeO_2]_{monomer}$, and as octamers, $[GeO_2]_{octamer}$

$$[GeO_2] = [GeO_2]_{monomer} + [GeO_2]_{octamer} \quad (8)$$

The total concentration of monomer is given by

$$[GeO_2]_{monomer} = [Ge(OH)_4] + [Ge(OH)_3O^-] \quad (9)$$

while the total concentration of germania nanoparticles is a sum of all the neutral and charged species

$$[GeO_2]_{octamer} = 8\sum_{i=1}^{n}[Ge_8O_{(11+i)}(OH)_{(9-i)}^{(i-1)-}],\ n = 1,2,...,9 \quad (10)$$

Last, the electroneutrality of the solution is accounted for by

$$0 = [TPA^+] + [H^+] - [OH^-] - [Ge(OH)_3O^-] - \sum_{i=1}^{n}(i-1)[Ge_8O_{(11+i)}(OH)_{(9-i)}^{(i-1)-}] \quad (11)$$

The combined sets of equilibrium equations and molar balances (eqs 2, 3, and 5−11) result in a system of three equations and three unknowns that are solved simultaneously using Newton's method to give the pH and individual concentrations of species as a function of the total germania concentration.

4. Results and Discussion

(A) Critical Aggregation Concentration. The phase behavior of germania in aqueous solutions was studied using pH, conductivity, and SAXS measurements. Incremental amounts of germanium (IV) ethoxide were added to basic solutions of composition X M^+OH^-/9500 H_2O, where M^+ is a monovalent cation. Various inorganic and organic cations were utilized in this study; however, tetrapropylammonium (TPA^+), the organic structure-directing agent employed in the synthesis of the zeolite ZSM-5, was chosen to develop the germania phase diagram.

Figure 2 shows the results of germania addition to solutions of varying alkalinity. Germanic acid, $Ge(OH)_4$, obtained from the hydrolysis of germanium (IV) ethoxide, dissociates at high pH, consuming OH^- and lowering the solution pH (see Figures 2b and 7). The conductivity is proportional to the concentration of ions in solution weighted by the respective ionic mobility.[43,45] Although the dissociation reaction generates charged $Ge(OH)_3O^-$ species that lead to positive changes in conductivity, the reduction of OH^- ions results in a net decrease in conductivity due to its smaller size and hence larger ionic mobility. Plots of conductivity versus $[GeO_2]$ in Figure 2a reveal a linearly decreasing trend that abruptly changes slope at a given germania concentration. Such behavior was recently observed in silica solutions, where it was shown that silica self-assembles at a specific silica concentration, termed the critical aggregation concentration (CAC),[46−48] leading to nanoparticles. The CAC for germania, analogous to silica, occurs at GeO_2/TPAOH = 1, which is the equivalence point for the acid−base reaction in eq 2. Figure 2b plots $[OH^-]$ versus $[GeO_2]$ scaled by the total TPAOH concentration. All experimental curves converge at a 1:1 GeO_2/OH^- molar ratio, thus creating two phases: region I containing germania monomers and/or oligomers and region II containing nanoparticles in equilibrium with soluble germania. At higher germania concentrations, particle aggregates form a third phase labeled region III. The onset of nanoparticle aggregation is accompanied by a shift from a clear solution to an opaque, white solution (see inset of Figure 3a). The transition between regions II and III is approximate as it was obtained through visual inspection of a small number of samples.

A solution with composition 9 TPAOH/Y GeO_2/9500 H_2O was analyzed by SAXS at varying germania concentrations (see Figure 3). Prior to the CAC (i.e., $Y < 9$), there are no particles present, as evidenced by the absence of a scattering signal; however, above the CAC (e.g., $Y = 20$), there are distinct SAXS patterns, indicating the presence of small particles (<2 nm) in solution. Increasing the concentration of GeO_2 ($Y = 40$, 60) results in an upturn of intensity at low q-values, thus signifying

(44) Pokrovski, G. S.; Schott, J. *Geochim. Cosmochim. Acta* **1998**, *62*, 1631.

(45) Castellan, G. W. *Physical Chemistry*, 3rd ed.; Addison-Wesley: Reading, MA, 1983.

(46) Fedeyko, J. M.; Rimer, J. D.; Lobo, R. F.; Vlachos, D. G. *J. Phys. Chem. B* **2004**, *108*, 12271.

(47) Fedeyko, J. M.; Vlachos, D. G.; Lobo, R. F. *Langmuir* **2005**, *21*, 5197.

(48) Rimer, J. D.; Fedeyko, J. M.; Vlachos, D. G.; Lobo, R. F. *Chem.—Eur. J.* **2006**, *12*, 2926.

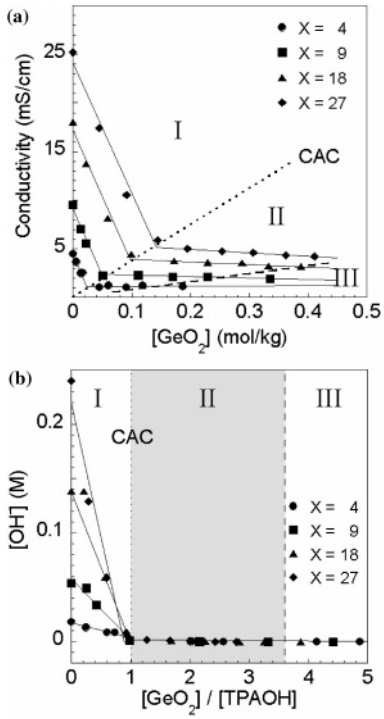

Figure 2. Plots of (a) conductivity and (b) $[OH^-]$ as a function of the total $[GeO_2]$ for solutions of composition *X* TPAOH/9500 H_2O (with $X = 4$, 9, 18, and 27). In panel b, the hydroxide concentration was obtained from pH measurements, and the *x*-axis is scaled by the total concentration of TPAOH (labeled as [TPAOH] in this paper). Solid lines are linear regression fits to data prior to and following the CAC. Dotted lines indicate the transition from regions I to II at the CAC, while dashed lines are approximates of the transition from regions II to III.

a third population of larger particles (>50 nm). The peak at $q = 2$ nm^{-1} confirms that GeO_2 nanoparticles are present along with the larger, condensed germania species, which may be aggregates of the nanoparticles.

SAXS patterns were fit with various geometric form factors, such as uniform sphere, cylinder, and ellipsoid models, using the software provided by the National Institute of Standards and Technology.[49] It was found that the best fit to the experimental data was that of a sphere with a diameter of 1.2 nm. Figure 3b shows the model fit (solid line) to the experimental data; the inset is the corresponding pair distance distribution function (PDDF, P(R)) (i.e., the Fourier transformation of the SAXS pattern from reciprocal space to real space—a method developed by Glatter[50] and discussed in greater detail in ref 43). The shape of the PDDF is indicative of the particle's size, for which we find the maximum length scale of 1.2 nm in excellent agreement with the diameter obtained from the spherical form factor model. In addition, the PDDF shape contains information on the particle morphology and polydispersity, which will be discussed in greater detail in section 4C.

(B) Effects of Monovalent Cations. It has been shown in silica solutions that alkali metals and TAA cations do not affect the CAC, size, and shape of the nanoparticles but do influence the transition from region II to III.[47] Here, we analyze germania nanoparticle self-assembly in the presence of inorganic and organic cations—looking specifically at the effects of cation identity on the CAC and size of the nanoparticles. We have

(49) NIST SANS Analysis Package, available at www.ncnr.nist.gov/programs/sans/manuals/data_anal.html.

(50) Glatter, O.; Kratky, O. *Small-Angle x-Ray Scattering*; Academic Press: New York, 1982.

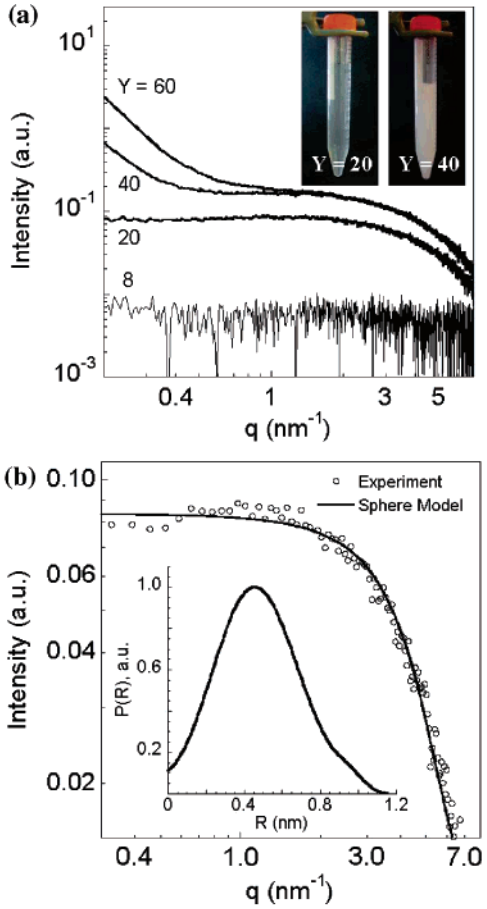

Figure 3. SAXS analyses of 9 TPAOH/*Y* GeO_2/9500 H_2O solutions with $Y = 8$, 20, 40, and 60. (a) Plots of intensity vs scattering vector, **q**, with the inset showing pictures of the solution in region II ($Y = 20$) and region III ($Y = 40$). (b) Analysis of germania nanoparticles, $Y = 20$, where the raw data (symbols) are modeled with a spherical form factor and a hard sphere structure factor (solid line). The inset contains the PDDF of the SAXS pattern, showing a maximum particle dimension of 1.2 nm.

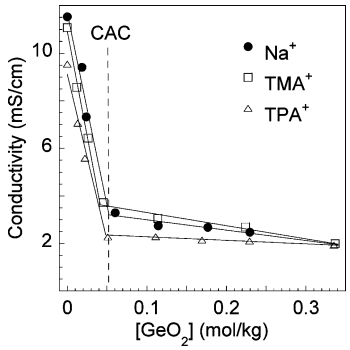

Figure 4. Conductivity measurements with germania addition to solutions of molar composition 9 M^+OH^-/9500 H_2O with M = Na^+, TMA^+, or TPA^+. Solid lines are linear regression fits to the data prior to and following the CAC.

chosen cations typically employed in zeolite syntheses: Na^+, TMA^+, and TPA^+. Figure 4 compares the CAC curves for these solutions showing that nanoparticle self-assembly occurs at a 1:1 molar ratio of GeO_2/OH^- regardless of the cation. The initial conductivities in Figure 4 are shifted in magnitude according to the cation ionic mobility, λ_i, which increases as $\lambda_{TPA^+} < \lambda_{TMA^+} < \lambda_{Na^+}$.[45] Linear regression (solid lines) of the curves prior to the CAC indicate that the slopes are approximately equal for all cations (due to OH^- removal being the primary contribution to

Table 1. Diameters of Spherical Form Factor Fits to SAXS Patterns of Solutions with Composition *X* M^+OH^-/*Y* GeO_2/9500 H_2O/4*Y* EtOH

M^+	*X* OH^-	*Y* GeO_2	*D* (nm)
Na	9	20	1.5
TMA	9	20	1.2
TPA	4	20	1.2
	9	20	1.2
	18	30	1.2
	27	35	1.1

changes in conductivity), whereas differences in slope following the CAC are most likely related to cation−nanoparticle interactions.

The sizes of Na^+, TMA^+, and TPA^+ nanoparticles at varying compositions were obtained from spherical form factor fits of the SAXS patterns. The resulting diameters, listed in Table 1, are ∼1.2 nm and independent of both the solution pH and the total germania concentration. Nanoparticles formed with Na^+ appear larger (1.5 nm); however, this difference is most likely caused by the adsorbed cation on the surface of the germania nanoparticle. Similar effects were observed for silica nanoparticles that have a core−shell structure[46] with a core composed of hydrated silica and a shell of adsorbed cation (i.e., the Stern layer of counterions expected from electrostatic theory[51]).

To understand the differences in scattering among varying cations, we must consider the intensity from small-angle scattering

$$I(q) = n_p \Delta\rho^2 V^2 P(q) S(q) \tag{12}$$

where n_p is the number density of nanoparticles, V is the particle volume, $P(q)$ is the form factor, $S(q)$ is the structure factor, and $\Delta\rho$ is the contrast (defined as the difference between particle and solvent scattering length density, SLD). The SLD in X-ray scattering is based on a molecule's electron density. Organic molecules, such as TAA cations, have SLDs similar to that of the water and exhibit little scattering. Inorganic cations, such as Na^+, have a much higher electron density and thus readily scatter X-rays. Given that germania species carry a negative charge at high pH due to the dissociation reactions, the cations are attracted to the particle surface. Thus, the increased size of Na^+ nanoparticles is caused by the adsorbed layer of Na^+, which has an ionic diameter of 0.99 Å that varies depending on the degree of hydration[52] (obtaining exact dimensions would require direct comparisons between SAXS and small-angle neutron scattering).

(C) Germania Nanoparticle Structure. Identifying the connectivity of germania nanoparticles by methods such as ^{73}Ge NMR or electron microscopy is impractical since the former is not readily available and single-particle imaging from the latter is a challenging task. Studies, such as those by Li et al.,[31] report that the cubic octamer is commonly formed in aqueous germania solutions. In addition, Villaescusa et al.[53] showed by ^{19}F NMR that in neutral, fluorous analogs of the solution studied here with tetraethylammonium (TEA) cations (i.e., molar compositions of GeO_2/0.5 TEAOH/0.5 HF/2.7 H_2O), germania forms D4R units. Here, we use the SAXS patterns in Figure 3b to gain insight into the germania nanoparticle structure—specifically focusing on PDDF analyses to distinguish the particle morphology.

The general shape of the PDDF (inset of Figure 3b) can be characterized as one of four possible geometries: monodisperse spheres, polydisperse spheres, ellipsoids, or cubes. Form factor analyses of SAXS patterns with an ellipsoid model result in *a*- and *b*-axis dimensions that are approximately equal and hence indistinguishable from the uniform sphere geometry. Therefore, we are left with three viable possibilities. First, we consider monodisperse spheres, which have an analytical equation for the PDDF given by

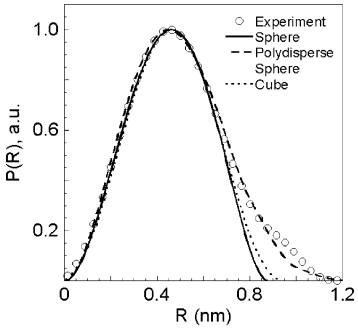

Figure 5. PDDF analysis of nanoparticles formed in a 9 TMAOH/40 GeO_2/9500 H_2O/160 EtOH solution, with the experimental PDDF (symbols), the analytical sphere model with a radius of 0.45 nm (solid line), a polydisperse sphere model of radius 4.6 ± 0.9 Å (dashed line), and the theoretical cube with an edge length of 0.35 nm (dotted line). The polydisperse sphere model was fit according to the protocol reported in ref 43.

$$P(R) = \frac{3}{4\pi}\frac{r^2}{R^2}\left(2 - \frac{3}{2}\frac{r}{R} + \frac{r^3}{8R^3}\right) \tag{13}$$

where r is the particle radius and R is the spatial parameter used in the calculation of the PDDF. Figure 5 compares the monodisperse sphere model to experiment, where a radius of 4.5 Å provides the best fit. The experimental PDDF is more elongated at larger *R*-values, which is oftentimes a characteristic of sample polydispersity. To test this, the experimental curve was fit with a polydisperse sphere model by first assuming a Gaussian distribution, then following the procedure outlined in ref 43. The resulting polydispersity is 0.19 with an average radius of 4.6 ± 0.9 Å, where the uncertainty is the standard deviation of the Gaussian distribution—a value that is less than a single Ge−O−Ge bond length of 3.2 Å.

Glatter compared the PDDFs of a monodisperse sphere and a cube, showing that the cubic geometry results in the elongation of curve at higher *R*-values. Such behavior may explain the deviation observed between the spherical model and the experimental curves in Figure 5. Unlike the sphere, an analytical form of the PDDF is not available for the cube; however, it is possible to calculate a theoretical SAXS pattern in reciprocal space and perform the Fourier transform to obtain the cubic PDDF. The form factor for a cube with edge length, *a*, is given by[54]

$$P(q,a) = \frac{2}{\pi}\int_0^{\pi/2}\int_0^{\pi/2} \left[\frac{\sin(qa\sin\alpha\cos\beta)}{qa\sin\alpha\cos\beta}\frac{\sin(qa\sin\alpha\sin\beta)}{qa\sin\alpha\sin\beta}\frac{\sin(qa\cos\alpha)}{qa\cos\alpha}\right]^2 \sin\alpha\, d\alpha\, d\beta \tag{14}$$

The best fit for the cubic PDDF is when a = 3.5 Å (see dotted line in Figure 5). The cube provides a slightly better fit at larger

(51) Hiemenz, P. C.; Rajagopalan, R. *Principles of Colloid and Surface Chemistry*, 3rd ed.; Marcel Dekker: New York, 1997.

(52) *CRC Handbook of Chemistry and Physics*, 77th ed.; CRC Press: Boca Raton, FL, 1996.

(53) Villaescusa, L. A.; Wheatley, P. S.; Morris, R. E.; Lightfoot, P. *Dalton Trans.* **2004**, 820.

(54) Lindner, P.; Zemb, T. *Neutrons, X-rays, and Light Scattering Methods Applied to Soft Condensed Matter*, 1st ed., North-Holland Delta Series; Elsevier: Amsterdam, 2002.

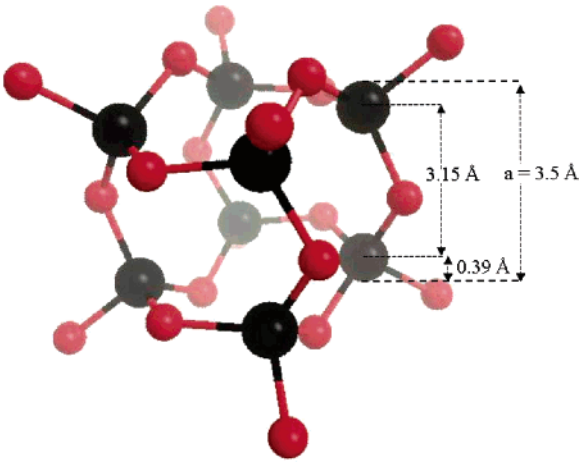

Figure 6. Diagram of the germania octamer with germanium (black) and oxygen (red) atoms (hydrogen atoms are omitted for clarity). The Ge−O bond length is 1.74 Å,[55] and the Ge−O−Ge bond angle is 130°; thus, the Ge−O−Ge distance is 3.15 Å. The ionic radius for Ge^{+4} with four-coordination is 0.39 Å;[52] therefore, the edge length, *a*, for the germania cube measured in SAXS experiments can vary from 3.2 to 4.0 Å. A cubic geometry with $a = 3.5$ Å provided the best fit to the PDDF in Figure 5.

R-values but is virtually indistinguishable from the sphere. At such small length scales, the sphere and cube have approximately equal surface areas and thus exhibit similar scattering patterns.

Inference of the Ge−O−Ge bond length by SAXS can vary depending on the ionic radius of germanium (i.e., Ge−O−Ge distance is 3.2−4.0 Å) since X-rays scatter from the electron cloud of Ge. The cubic PDDF results in an edge length of 3.5 Å, which is in excellent agreement with the dimensions of the Ge−O−Ge bond distance (see Figure 6 for schematic diagram of a germania cubic octamer with labeled dimensions). However, we cannot rule out the possibility that some degree of polydispersity exists, perhaps caused by ring opening of D4R units to form structures, such as five-membered rings. It is also possible that elongation of the PDDF at higher *R*-values is attributed to interparticle interactions (i.e., $S(q)$ contributions to the scattering); however, based on the absence of distinct interaction peaks in Figure 3a, we do not expect these contributions to be significant.

(D) Chemical Equilibrium Model. The germania phase diagram is plotted in terms of pH versus the total germania concentration in Figure 7. The phase diagram consists of three distinct regions: region I containing germania monomers and/or oligomers, region II containing octamers in equilibrium with soluble germania, and region III containing octamers, soluble germania, and condensed and/or aggregated germania nanoparticles. Here, we assume that the soluble germania is in the form of monomers that can undergo a single dissociation. The model equations (see section 3) are solved simultaneously to calculate the changes in species concentrations and pH at a given $[GeO_2]$.

Equilibrium constants for germania dissociation and condensation are known (or estimated) from the literature, with the exception of the dissociation constants for the germania octamer, pK_{as}^{i}, which became the adjustable parameters in the model. It is known for inorganic oxides that an increase in coordination number results in more acidic hydroxyl groups.[56] In addition, the acidity generally decreases with subsequent dissociations; thus, one may expect the germania cube with its eight ≡GeO−H bonds to have the following trend: $pK_{as}^{1} \leq pK_{as}^{2} \leq ... \leq pK_{as}^{8}$. However, in the absence of experimental data for the ΔG of each

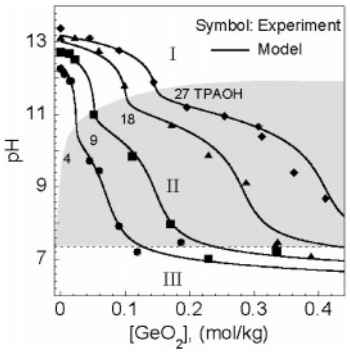

Figure 7. Germania phase diagram with experimental points (symbols) for solutions of varying alkalinity (i.e., *X* TPAOH). The results of the chemical equilibrium model are plotted (solid lines), region II is shaded for visual comparison, and the boundary between regions II and III (dashed line) is an approximation drawn according to visual observation of destabilized, or aggregated, GeO_2 octamers (i.e., appearance of turbid samples).

dissociation, we assume that all dissociations are equal (i.e., $pK_{as}^{1} = pK_{as}^{2} = ... = pK_{as}^{i}$), similar to models of silica nanoparticles.[57]

We fit the $X = 9$ TPAOH data in Figure 7 to a single pK_{as}^{i} value beginning with $i = 1$ up to a maximum of $i = 8$. The residual for each condition was calculated by comparing differences between experiment and model (i.e., $R = \sum_i (pH_{expt,i} - pH_{model,i})^2$). It was found that the best fit occurs when only three ≡GeO−H− groups dissociate (i.e., $i = 1, 2, 3$) with $pK_{as}^{i} = 7.1$. This equilibrium constant was then used to predict the remaining TPAOH curves, the results of which are shown as solid lines in Figure 7. The value of pK_{as}^{i} is an average overall for ≡GeO−H− groups, but the possibility of more than three hydroxyl groups dissociating should not be ruled out, although the presence of three negative sites does agree with Cotton and Wilkinson who state that $\{[Ge_8(OH)_4]_8(OH)_3\}^{3-}$ is a common species in aqueous germania solutions.[38] Finally, we should note that the model holds strictly in regions I and II and, within its approximations, is plotted in region III to describe the monomer−octamer equilibrium for visual purposes.

Figure 8 depicts concentration profiles of monomer and octamer species as a function of the total germania. The only species present in region I is that of the negatively charged monomer. At the CAC, there is a small amount of germanic acid, $Ge(OH)_4$, that leads to the self-assembly into octamers. Following the CAC, there is a drop in the concentration of $Ge(OH)_3O^-$ species due to the significant decrease in solution pH. With subsequent germania addition, there is a second inflection point in the curves of Figure 7 that corresponds to the concurrent increase in $Ge(OH)_4$ and decreases in charged octamer (i.e., $Ge_8O_{15}(OH)_5^{3-}$). Figure 8b contains concentration profiles of the dissociated octamer species showing that, initially, $Ge_8O_{15}(OH)_5^{3-}$ is the principal species, but as the pH is lowered, there is a mixture of octameric species present in solution of varying degrees of deprotonation.

(E) Comparison of GeO_2 and SiO_2 Nanoparticles and Phase Behavior. In sections 4A−D, general analogies were made between solutions of germania and silica. From these and previous studies, it was observed that both GeO_2 and SiO_2 exhibit a CAC at an oxide/TPAOH molar ratio of one, above which spontaneous self-assembly occurs. The resulting nanoparticle size and shape are independent of the cation identity; and although it cannot be conclusively determined from SAXS studies alone, the germania

(55) Ingri, N.; Lundgren, G. *Acta Chem. Scand.* **1963**, *17*, 617.
(56) Sefcik, J.; McCormick, A. V. *AIChE J.* **1997**, *43*, 2773.
(57) Rimer, J. D.; Lobo, R. F.; Vlachos, D. G. *Langmuir* **2005**, *21*, 8960.

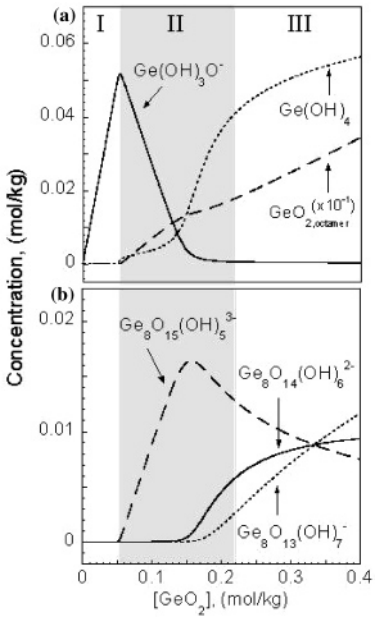

Figure 8. Concentration profiles of germania monomer and octamer species from model calculations with a composition of 9 TPAOH/9500 H_2O and pK_{as}^{i} = 7.1. (a) Plots of the neutral and negatively charged monomer species along with the total concentration of germania octamers (scaled by a factor of 10 for clarity). (b) Plots of the charged octamer species as a function of germania addition. It was found that a maximum of three octamer dissociations gave the best fit to the data in Figure 7.

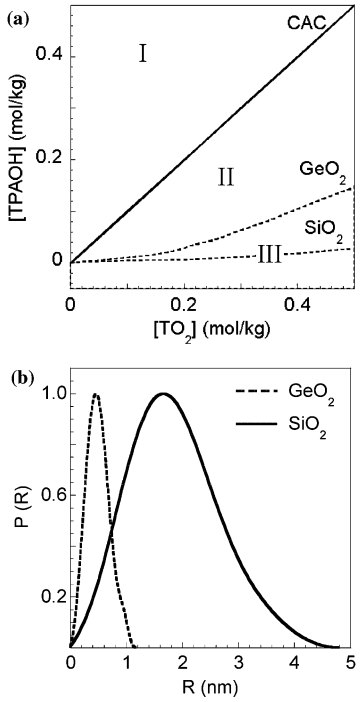

Figure 9. Comparison of pure germania and silica aqueous solutions. (a) Plot of the initial hydroxide concentration vs [TO_2] showing regions I−III for T═Ge and Si. The CAC is the line separating regions I and II and has a slope of one. Dashed lines are approximations based on visual inspection of destabilized SiO_2 and GeO_2 solutions, signifying the onset of region III. (b) PDDFs of GeO_2 octamers and SiO_2 nanoparticles, analyzed at the composition 9 TPAOH/40 TO_2/9500 H_2O/160 EtOH.

octamers most likely possess a core−shell structure analogous to those formed in silica.[38,41−43]

In Figure 9a, the TPAOH concentration is plotted against the concentrations of GeO_2 and SiO_2 to compare their respective phase behavior. As previously noted, the CAC line separating regions I and II is identical for germania and silica. The dissociation constants for the germania octamer (pK = 7.1) and silica nanoparticle (pK = 8.4) species reveal the former to be more acidic. Therefore, the transition from region II to III occurs at a much lower pH for GeO_2 (pH = ∼7) as compared to solutions of SiO_2 (pH = ∼10). In addition, there are distinct differences in their material properties. Silica nanoparticles agglomerate in region III to form a slightly opaque sample-spanning gel, while germania forms a milky white fluid. Second, and perhaps most strikingly, the silica nanoparticle size strongly depends on solution pH, while GeO_2 octamers are constant over the entire pH range studied. Silica nanoparticles have either an oblate ellipsoid or polydisperse sphere morphology,[47] while the germania particles are cubic octamers of much smaller size. Figure 9b emphasizes some of these differences by comparing the PDDFs of both nanoparticles for a given composition, where it is observed that SiO_2 particles are nearly 4 times larger. It is likely that the driving force for smaller GeO_2 particles is due to its lower equilibrium constant for condensation (eq 5, pK_c = −1.02) as compared to that of silica.

$$\mathrm{Si(OH)_4} \overset{K_c}{\longleftrightarrow} \frac{1}{n}\mathrm{Si}_n\mathrm{O}_{4n-m}\mathrm{H}_{4n-2m} + \frac{m}{n}\mathrm{H_2O} \qquad (15)$$

The latter has a much higher value of −2.98,[57] thus leading to particles with n = 200 − 400. Germanium solutions in region II are true equilibrium compositions (i.e., a solid will not be formed), while silica solutions in region II are metastable and will eventually lead to the formation of solids (such as zeolites).

The CAC and phase diagrams for germania and silica are both captured reasonably well by a simple chemical equilibrium model. In this study, we have assumed that all soluble germania is in the form of monomers capable of undergoing only a single dissociation; however, it is known that $Ge(OH)_2O_2^{2-}$ species are present at high pH.[38,44,58,59] We find that inclusion of the second monomer dissociation for germania follows the exact trends reported in ref 57 for aqueous silica solutions. The second dissociation leads to a slight underprediction of the pH in region I at high alkalinity (e.g., X > 9 TPAOH). For silica, it was shown that a more complete model requires the inclusion of oligomers. Such may be the case with germania, but without experimental methods of measuring soluble germania species (e.g., ^{73}Ge NMR), these analyses are outside the scope of this study.

5. Conclusion

We present analyses of germania phase behavior in basic aqueous solutions showing the spontaneous self-assembly of germania into nanoparticles at the CAC. The phase diagram shows three distinct regions: region I containing germania monomers/oligomers, region II containing nanoparticles, and region III comprised of condensed or aggregated germania in equilibrium with monomers and octamers. A thermodynamic model was used to capture the phase diagram as a function of germania concentration, with the equilibrium constant for ≡GeO−H dissociation, pK_{as}, as the only adjustable parameter. Analogous to silica, the CAC occurs at a 1:1 ratio of GeO_2/OH^- corresponding to the germania solubility. The resulting germania nanoparticles are nearly 4 times smaller and more acidic (pK_{as} = 7.1) than their silica counterparts. The germania nanoparticle size is independent of solution pH and the monovalent cation used to supply hydroxide to solution. SAXS analyses reveal that

(58) Ingri, N. *Acta Chem. Scand.* **1963**, *17*, 597.
(59) Ingri, N.; Schorsch, G. *Acta Chem. Scand.* **1963**, *17*, 590.

the nanoparticle morphology is best described as either a sphere or a cube—both of which have similar dimensions of ~1 nm. We propose that the nanoparticle structure is the cubic octamer, $Ge_8O_{12}(OH)_8$, based on the SAXS studies presented here and previous reports showing D4R formation in pure germania and [Ge,Si]-zeolites. This study is part of an ongoing effort toward understanding the role of heteroatom substitution for Si in zeolites—more specifically, the effects of Ge on the structure direction of zeolitic frameworks[22,36] and the kinetics/mechanism of crystallization.[21,23]

Acknowledgment. This work was funded in part by the National Science Foundation Nanoscale Interdisciplinary Research Team (NIRT) under Grant CTS-0103010 and by the American Chemical Society Petroleum Research Fund under Grant 43464-AC10.

LA062828Q